RSC Advances

PAPER

View Article Online
View Journal | View Issue

Cite this: *RSC Adv.*, 2025, **15**, 7742

Facile preparation of fluorescent carbon dots from water caltrop shells and their application in amikacin sensing†

Yi Zhang, ‡ Ping Dong, ‡ Xin Chen, ‡ Jin Wang, Yun Zhang * and Bowen Liu *

Received 21st January 2025
Accepted 5th March 2025

DOI: 10.1039/d5ra00501a

rsc.li/rsc-advances

Amikacin (AMK) effectively treats infections from Gram-negative bacilli and penicillin-resistant *Staphylococcus aureus*. However, prolonged administration of AMK may result in adverse effects such as nausea, headache, ototoxicity, and hearing loss, necessitating a reliable detection method. Carbon dots (CDs), known for their excellent optical properties, are a promising fluorescent probe. This study developed cost-effective, eco-friendly WCS-CDs from water caltrop shells using a simple hydrothermal process for AMK detection and analysis. The WCS-CDs emitted at 380 nm when excited at 290 nm and demonstrated selective sensitivity to AMK, with fluorescence quenching linearly related to AMK concentration from 1.5 to 21.5 μg mL^{-1} ($Y = 376.98 + 57.75X$, $R^2 = 0.992$). This simple method allows for accurate AMK quantification in real samples, achieving recoveries of 95.58–105.63%.

Introduction

Amikacin (*O*-3-amino-3-deoxy-α-D-glucopyranosyl-(1 → 4)-*O*-[6-amino-6-deoxy-α-D-glucopyranosyl-(1 → 6)]-*N*′-(4-amino-2-hydroxy-1-butyl)-2-deoxy-L-streptamine, AMK, Fig. 1) is an aminoglycoside antibiotic characterized by its high efficacy and broad-spectrum antibacterial activity, particularly effective against infections in the urinary tract, brain, and lungs.[1–3] AMK is typically presented as a white or nearly white crystalline that is readily soluble in water and has been employed in the treatment of tuberculosis for several decades. The mechanism of action of amikacin involves the inhibition of bacterial protein synthesis by disrupting the integrity of the bacterial cell wall and membrane upon binding to the ribosome, ultimately resulting in bacterial cell death and exerting its antibacterial effects.[4–6] Several clinical observations have indicated that long-term AMK treatment can lead to hearing loss and kidney side effects, making sensitive and reliable monitoring essential.[7–9] Current detection methods, such as high-performance liquid chromatography,[10,11] Fourier transform infrared spectroscopy, and surface enhancement of Raman scattering analysis, are time-consuming and require complex equipment.[12–14] Therefore, there is an urgent need for a simple, quick, and cost-effective method for AMK detection.

Carbon nanomaterials are materials predominantly composed of carbon, characterized by their nanoscale dimensions ranging from 1 to 100 nm. This category primarily includes fullerenes, carbon nanotubes, graphene, and carbon dots.[15–19] CDs, in particular, represent a novel class of luminescent nanomaterials that have garnered significant attention in recent years due to their size below 10 nm, facile synthesis, cost-effectiveness, tunable luminescence, stability, high water solubility, low toxicity, and other advantageous properties.[20] In essence, carbon dots integrate the optical properties of quantum dots with the electronic characteristics of carbon nanomaterials.[21–24] Due to their unique properties, CDs are versatile materials that can be utilized in a wide range of applications, including drug and gene delivery, bioimaging, photodegradation, and the fabrication of three-dimensional printed patterns.[25–31] The precursors for the synthesis of

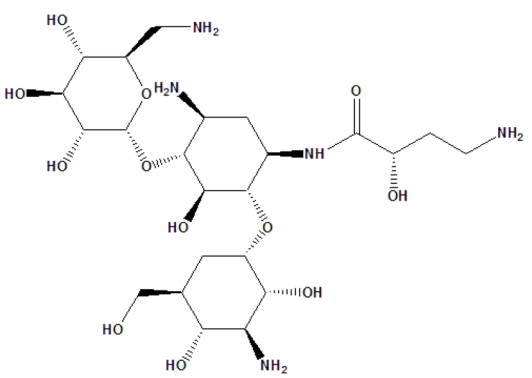

Fig. 1 Molecular structure of amikacin.

School of Medical Technology, Xinxiang Medical University, Xinxiang 453003, Henan, P. R. China. E-mail: zhangyun@xxmu.edu.cn; liubowen309@163.com; Fax: +86 373 3029977; Tel: +86 373 3029977

† Electronic supplementary information (ESI) available. See DOI: https://doi.org/10.1039/d5ra00501a

‡ The first three authors contribute equally.

carbon dots have become increasingly diverse, with researchers frequently opting for biomass resources derived from the natural environment. The precursors for carbon dots synthesis become even more diverse, and researchers are apt to select biomass resources from the natural world.[32–34]

CDs serve as biomarkers and probes, exhibiting excellent biocompatibility and minimal cytotoxicity. The excellent performance will enable its application in the medical domain, the imaging of biological cells and biological tissues, which circumvents the weakness of conventionally available fluorescent dye molecules. Researchers widely explored different ways to synthesize CDs with different properties. For instance, Hu *et al.*[35] synthesized green fluorescent carbon dots with Eosin Y and branched polyethyleneimine. It provides a novel "turn-on" fluorescence sensor for the detection of H_2O_2 and glucose. Wu *et al.*[36] used carbon dots as cross-linking agents for egg white in a dilute aqueous solution. The resulting carbon dots crosslinked egg white hydrogel demonstrated tensile strength comparable to that of skin tissue, thus indicating its potential for utilization as a wound dressing material. Dai *et al.*[37] developed ultra-small carbon dots loaded with zinc single-atom nanozyme to promote wound healing by nanocatalytic treatment. Dong *et al.*[38] evaluated the visible light-activated antibacterial function of carbon-TiO_2 hybrid quantum dots, with the results showing the effective killing of Gram-positive and Gram-negative bacteria. Najmalden Ghaibullah Ghaibullah *et al.*[39] immobilized carbon dots from Elaeagnus angustifolia fruits on chitosan and glass microbeads' surfaces. The study showed that the carbon dots could be used as carbon-based nanomaterials in antibacterial surface preparation once immobilized. Dos Santos de Almeida *et al.*[40] presented a novel tissue equivalent dosimeter carbon dots-based as an ionizing radiation sensor and provided valuable insights into the potential applications of carbon dots in different fields. Wang *et al.*[41] synthesized novel carbon dots using diaminomaleonitrile and Boc-D-2,3-diaminopropionic acid. The as-prepared carbon dots were utilized in fluorescent ink in anti-counterfeiting measures and successfully utilized in cell imaging.

This study demonstrates the low-cost production of carbon dots (WCS-CDs) through a simple one-step hydrothermal reaction using water caltrop shells. Annually produced as waste, WCS is rich in lignin, flavonoids, polyphenols, alkaloids, and other active ingredients, which act as precursors for carbonaceous materials that improve the fluorescence of nanocarbon materials.[42,43] The hydrothermal process converts the organic content of WCS into carbonaceous nanoparticles. Recently, discarded WCS has gained significant research attention.[44,45] The WCS-CDs emitted at 380 nm when excited at 290 nm and demonstrated selective sensitivity to AMK. The research results provide new technical approaches and theoretical frameworks for the detection of amikacin, holding significant implications for human health.

Experimental

Reagents

Water caltrop shells were used as precursors to prepare fluorescent carbon dots. Ultrapure water was used throughout the experiment. The amikacin, L-arginine, DL-arginine, L-cysteine, L-cystine, L-*tert*-leucine, kanamycin, penicillin–streptomycin–gentamicin solution, neomycin sulfate, and spectinomycin reagent were of analytical grade. A series of Britton–Robinson (BR) buffer solutions with a pH range of 1–11. BR buffer, Tris–HCl buffer, KH_2PO_4–NaOH buffer, PBS buffer, Na_2HPO_4–citric acid buffer, Na_2HPO_4–NaH_2PO_4 buffer, and $NaHPO_4$–KH_2PO_4 buffer are formulated to optimize the WCS-CDs–AMK system. The BEAS2B cells (a human normal lung epithelial cell line), the A549 cells (a human epithelial cell line derived from lung carcinoma tissue), and the BMDM cells (mouse bone marrow primary macrophage cells) obtained from the School of Medical Technology of Xinxiang Medical University were used in the experiments to detect the cytotoxicity and cell imaging of WCS-CDs. Human serum samples were obtained from the same institution, and lake and tap water were taken from the university water source to be used in real sample applications.

Characterizations

WCS-CDs were synthesized by a one-pot solvothermal method using an electric thermostatic drying oven (DHG-9140A, Yiheng Shanghai). The microstructure and size of the synthesized WCS-CDs were analyzed through high-resolution transmission electron microscopy (HRTEM, Tecnai G2 F20, FEI UK) with a voltage of 200 KV. The crystal structure of WCS-CDs was characterized by X-ray diffraction (XRD, Bruker D8 Advance) with a step size of 0.02°. The Fourier transform infrared spectroscopy (FTIR, Thermo Nicolet iS5) identified the presence of various functional groups. The elemental composition and molecular structure were analyzed through X-ray photoelectron spectroscopy (XPS, Thermo ESCALAB 250Xi) equipped with an Al Ka X-ray source, 150 W power, and 500 μm diameter beam spot. The ultraviolet-visible Spectrophotometer (T9S, PUXI Beijing) recorded the ultraviolet absorption spectra and the fluorospectrophotometer (F-7000, Hitachi Japan) recorded the fluorescence spectra of the WCS-CDs solution and WCS-CDs–AMK system.

Preparation of CDs

Water caltrop shells were collected from biomass waste, dried, and smashed into powder, subjected to hydrothermal treatment to produce water-soluble carbon dots. The optimal synthesis conditions of the WCS-CDs were optimized by evaluating the fluorescence intensity under various reaction temperatures, reaction times, and concentrations of reactants. Ultimately, the optimum reaction conditions of WCS-CDs were a reaction temperature of 250 °C, a reaction time of 2 hours, and a WCS concentration of 20 mg mL^{-1}. In brief, 0.2 g of water caltrop shells powder was dispersed in 10 mL of ultrapure water and then transferred into a 25 mL Teflon-lined stainless-steel autoclave for hydrothermal treatment at 250 °C for 2 h. After being cooled naturally, the resulting supernatant of the CDs solution was filtered using a 0.22 μm membrane filter and stored at 4 °C. An aqueous WCS-CDs suspension with a concentration of 3 mg mL^{-1} was prepared for dilution treatment in the subsequent spectroscopic characterizations and tests.

Procedure for amikacin detection

Unless specifically stated, the standard experimental conditions for the determination of amikacin are as follows: under optimal conditions, the WCS-CDs stock dispersion (3 mg mL^{-1}) is added to 0.5 mL Tris–HCl buffer solution to maintain a consistent pH of 7.4, and then the mixture is diluted with ultrapure water to a volume of 4 mL, resulting in a fixed CDs concentration of 15 μg mL^{-1}. The carbon dots aqueous solution was respectively combined with varying concentrations of amikacin solution, ranging from 0 to 21.5 μg mL^{-1}, to establish the concentration-dependent relationship. The mixture was thoroughly mixed, and the fluorescence spectra were recorded at an excitation wavelength (EX) of 290 nm.

Sample preparation

Human serum, tap water, and lake water were used as real samples to verify the feasibility of the constructed WCS-CDs for AMK analysis. To separate the proteins from the serum, the samples were centrifuged at 10 000 rpm for 15 min and the supernatant was collected. The lake water and tap water samples were filtered through a 0.22 μm microporous membrane to remove solid contaminants from the liquid for use. The final concentrations of AMK were 2 μg mL^{-1}, 8 μg mL^{-1}, and 14 μg mL^{-1}, respectively, and the constructed fluorescence sensor system was employed to detect AMK under optimal conditions.

Cell toxicity

BEAS2B cells (a human normal lung epithelial cell line) and A549 cells (a human epithelial cell line derived from lung carcinoma tissue) were employed to evaluate the cytotoxicity of CDs. In brief, BEAS2B and A549 cells were seeded in two separate 96-well plates at a density of 5×10^4 cells per well. They were cultured in RPMI-1640 medium (Servicebio, Serbia) containing 5% fetal bovine serum (FBS) (LONSERA, China) and 0.5% penicillin–streptomycin solution, and they were maintained in an incubator at 37 °C in a 5% CO_2 atmosphere for 12 h. To analyze cell viability upon treatment with WCS-CDs, the cells were re-incubated with the cell culture medium (100 μL per well) containing varying concentrations of CDs (3, 5, 10, 20, 30 μg mL^{-1}) for 20 h. The medium was removed and replaced with 100 μL of culture medium containing 5% MTT and was incubated for 4 h to release formazan crystals. Once the supernatant was removed, the formazan was dissolved by adding 150 μL DMSO per well. The number of viable cells was determined indirectly by measuring the light absorption value at 490 nm with an enzyme-linked immunoassay detector.

Cell imaging

BMDM cells (mouse bone marrow primary macrophage cells) were used for cellular imaging analysis to verify the biocompatibility and cellular uptake of WCS-CDs. Cells were cultured in RPMI medium (Cytiva, USA) supplemented with 5% fetal bovine serum (Gibco, USA) and maintained at 37 °C and 5% CO_2 in a humid atmosphere. WCS-CDs were added to the cell culture medium and co-incubated with BMDM cells for 24 h. The cells were then rinsed with PBS, the solution was discarded, and the cells were fixed by adding 1 mL of 4% paraformaldehyde. After 20 min, fluorescence images of the cells were captured using an inverted fluorescence microscope (Zeiss Axio Vert A1) with the following filter sets: blue light (excitation: 350–380 nm, emission: 420–460 nm), green light (excitation: 450–490 nm, emission: 510–560 nm), and red light (excitation: 530–560 nm, emission: 590–640 nm).

Results and discussion

Waste biomass can be converted into carbon nanomaterials by regulating the reaction conditions of synthetic reactions. WCS-CDs were prepared through a one-step hydrothermal process using water caltrop shells as the precursor. The treatment was conducted at 250 °C for 2 hours, with a WCS concentration of 20 mg mL^{-1}, yielding a quantum yield (QY) of 6.25%. Fig. 2 is the schematic diagram and flowchart of the system. WCS-CDs emitted bright blue fluorescence immediately under ultraviolet light irradiation, demonstrating the fluorescent feature of WCS-CDs. Nevertheless, the addition of amikacin results in a reduction in the fluorescence intensity of the WCS-CDs. The phenomenon is utilized as a detection method for AMK.

Fig. S1–S3† indicate that optimal synthesis conditions for WCS-CDs were determined by evaluating the fluorescence intensity under various conditions.

Characterization of CDs

The size distribution and morphology of CDs can be obtained through TEM analysis. Fig. 3a shows that WCS-CDs are

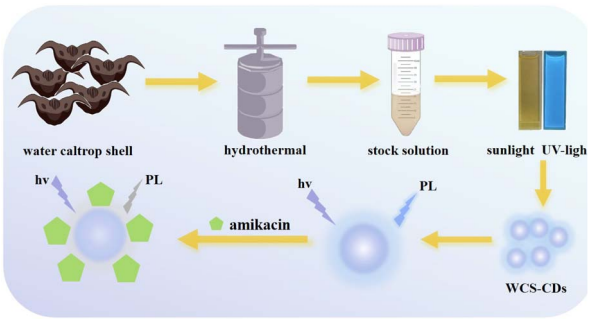

Fig. 2 Schematic diagram of the preparation and detection principle of the WCS-CDs.

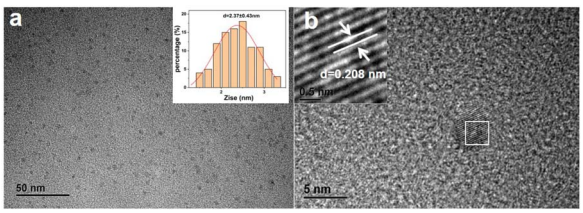

Fig. 3 (a) The TEM image of the WCS-CDs (inset: the particle size distribution); (b) the HRTEM image of the WCS-CDs.

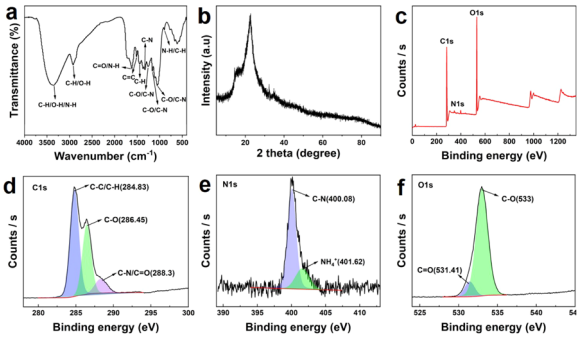

Fig. 4 (a) The FTIR spectrum of WCS-CDs; (b) the XRD spectrum of WCS-CDs; (c) the entire XPS scanning spectrum of the WCS-CDs, XPS high-resolution survey scan of C 1s (d), N 1s (e) and O 1s (f) of the WCS-CDs.

predominantly spherical with good dispersion and no significant aggregation. Their particle size (inset of Fig. 3a) ranges mainly from 1.41 to 3.31 nm, with an average diameter of 2.37 nm ($n = 100$). The HRTEM image in Fig. 3b reveals that the WCS-CDs exhibit a lattice structure, with a fringe spacing of 0.208 nm, attributed to the graphite carbon (100) plane.[46] This observation indicates the presence of sp^2-hybridized carbon layers within the nanoparticles.

Fig. 4a shows the FTIR spectrum of WCS-CDs. The broad absorption peak at a wavenumber of 3351.61 cm^{-1} is assigned to stretching vibrations of C–H, N–H, and O–H.[47] The peak at 2921.98 cm^{-1} is due to C–H stretching vibration and O–H telescopic absorption.[48,49] The peak at 1618.7 cm^{-1} is ascribed to C=O stretching vibration and N–H bending vibration.[50,51] C=C skeleton vibration is observed at a wavenumber of 1511.97 cm^{-1}.[49] The absorption peaks at 1450.14 cm^{-1} could be assigned to C–H bending vibration, while the range of wavenumbers between 1350–1000 cm^{-1} could be attributed to C–N stretching vibration absorption.[52] Additionally, the range of wavenumbers between 1300–1000 cm^{-1} could be ascribed to C–O stretching vibration.[53] The peak at 897.13 cm^{-1} indicates absorption of N–H and C–H out-of-plane bending vibrations. In summary, the structure of WCS-CDs suggests the presence of functional groups containing nitrogen and oxygen, which form the foundation of stability in aqueous solutions.

The XRD pattern of the WCS-CDs is shown in Fig. 4b. It exhibits a peak at 22.6°, which can be attributed to the reflection of the (002) planes of graphitic carbon.[49] The characterization results indicate effective and successful preparation of CDs *via* water caltrop shell precursor. The inconsistency results of XRD and TEM arise from the fact that CDs, due to their heterogeneous structure, can exhibit multiple lattice planes. The (100) plane observed in HRTEM represents the in-plane atomic arrangement, while the (002) plane in XRD reflects the interlayer stacking of graphitic sheets. The (002) plane is more prominent in XRD due to its strong diffraction intensity.

The XPS spectrum of WCS-CDs is presented in Fig. 4c. The characteristic peaks of carbon (C), oxygen (O), and nitrogen (N) are observed at 284.98 eV, 532.97 eV, and 400.13 eV, respectively, indicating that the sample primarily consists of C, O, and N elements.[54] To more precisely identify the elemental forms, the C 1s, N 1s, and O 1s spectra were fitted. As shown in Fig. 4d, there are three types of carbon in the C 1s spectrum, which are located at 284.83 eV, 286.45 eV, and 288.3 eV, corresponding to C–C/C–H, C–O, and C–N/C=O bonds.[55,56] The high-resolution O 1s spectrum in Fig. 4f mainly includes C=O (531.41 eV) and C–O (533 eV) bonds.[57] Additionally, the N 1s spectrum (Fig. 4e) can be fitted into C–N (400.08 eV) and NH_4^+ (401.62 eV) groups.[58] The FTIR and XPS results confirm that the surface of carbon dots contains a variety of functional groups, which enhance their dispersion and stability in aqueous solutions. It stabilizes the surface active sites as chromophores or co-chromophores, thereby strengthening the fluorescence activity of CDs.[57,59]

Optical properties of CDs

UV-vis spectrophotometer and fluorescence spectrophotometer investigated the optical properties of the WCS-CDs. Fig. S4(a)† illustrates the fluorescence intensity variation of WCS-CDs within the emission wavelength (EM) range of 370–420 nm. The results indicate that the fluorescence performance of the carbon dots reaches its maximum when EM = 380 nm. As illustrated in Fig. S4(b),† an evident shift in the emission peak towards a longer wavelength is observed as the excitation wavelength increases. This suggests that the carbon dots exhibit excitation wavelength-dependent properties, likely due to variations in dot size and surface states.[55] Fig. S4(c)† shows the optimal excitation and emission wavelength spectra for WCS-CDs. At an excitation wavelength of 290 nm, a strong fluorescence emission peak is observed at 380 nm, demonstrating the typical down-conversion fluorescence characteristics of CDs. The ultraviolet absorption spectrum of the WCS-CDs in Fig. S4(d)† shows a characteristic absorption peak at 272 nm, attributed to C=C and π–π* transitions.[51,60]

In the following section, Fig. 5a presents the fluorescence intensity of the carbon dots over 70 minutes, exhibiting

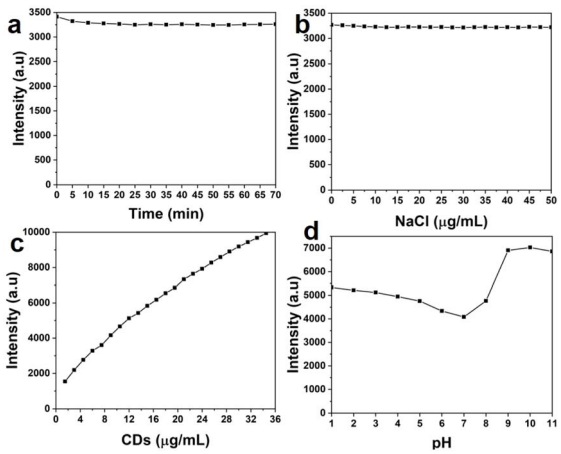

Fig. 5 (a) The stability of WCS-CDs at time ranges from 0 to 70 min; (b) the stability of WCS-CDs at different concentrations of NaCl; (c) fluorescence intensity of WCS-CDs with different concentrations; (d) the effects of the difference of pH (1–11) for the WCS-CDs.

negligible decline. This outcome signifies the presence of photobleaching resistance characteristics. Fig. 5b examines the fluorescence intensity stability of the carbon dots under varying ionic concentrations, demonstrating they still have strong stability in high ionic strength conditions. Fig. 5c shows the water stability of the WCS-CDs. There is a good increase in fluorescence intensity with the increase in the WCS-CDs concentration. The fluorescence intensity increase is not perfectly linear, the rate of increase in fluorescence intensity gradually slows down at higher concentrations due to the gradual influence of aggregation and self-absorption effects. Fig. 5d investigates the effect of different pH values on the fluorescence performance of the WCS-CDs, revealing significant pH dependence. To ensure stability in subsequent experiments, pH 7.4 (physiological pH) was selected as the experimental condition. The strong photoluminescence (PL) property enables the application of the WCS-CDs as a fluorescent probe in molecular biology science.[20]

In addition, the fluorescence lifetime of the WCS-CDs–AMK system was further determined, as shown in Fig. S5.† The fluorescence lifetime of WCS-CDs itself consisted of two parts, 0.42 ns (23.44%) and 2.71 ns (76.56%), and the average fluorescence lifetime of WCS-CDs was obtained as 2.17 ns by comparison and calculation. After adding AMK, the fluorescence lifetime comprised 0.18 ns (17.23%) and 2.19 ns (82.77%), reducing the lifetime to 0.21 ns. The addition suggested AMK may have enhanced the non-radiative relaxation process of fluorescent molecules, resulting in a shorter fluorescence lifetime and faster fluorescence decay.

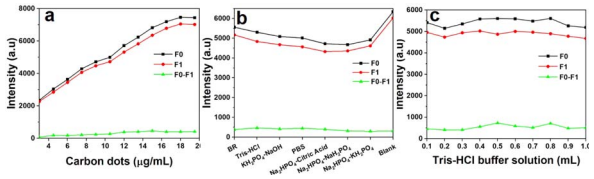

Fig. 6 (a) The optimal WCS-CDs concentration in the detection system; (b) the optimal type of buffer solution in the detection system; (c) the optimal buffer solution content in the detection system.

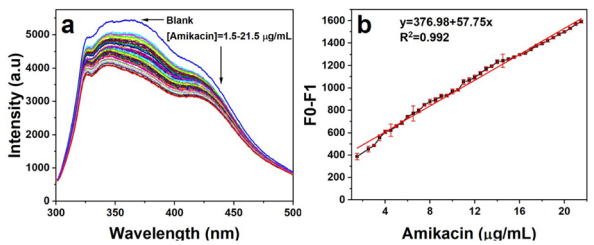

Fig. 7 (a) Fluorescence spectra of the WCS-CDs–AMK system at various AMK concentrations; (b) the standard curve of the WCS-CDs–AMK system.

Optimization of assay conditions

To enhance the detection capability of WCS-CDs for AMK, we optimized the carbon dots concentration (Fig. 6a), buffer type (Fig. 6b), and buffer volume (Fig. 6c) in the WCS-CDs–AMK system. F_0 represents the fluorescence intensity before AMK addition, while F_1 represents the intensity after AMK addition. By comparing the difference between F_0 and F_1, we determined that the optimal concentration of WCS-CDs is 15 μg mL^{-1}. The optimal buffer solution selected is Tris–HCl buffer solution with a volume of 0.5 mL in a 4 mL detection system.

Calibration curve and detection limit

Subsequently, a novel detection method for AMK was successfully prepared through a series of conditional optimization experiments, as illustrated in Fig. 7a. It is evident from the figure that the fluorescence intensity of WCS-CDs underwent a continuous quenching process when the concentration of AMK ranges from 1.5 to 21.5 μg mL^{-1}. Furthermore, it was observed that the concentration of AMK from 1.5 to 21.5 μg mL^{-1} exhibited a strong linear correlation with the quenched value of WCS-CDs fluorescence intensity (see Fig. 7b). The linear equation for this relationship is F_0–F_1 = 376.98 + 57.75[Q], with a high level of significance as indicated by the correlation coefficient of 0.992. The detection limit (LOD) was calculated using the formula:

$$\mathrm{LOD} = 3 \times (\sigma/k)$$

where σ represents the standard deviation of the blank measurements, and k is the slope of the calibration curve. In this study, the LOD was determined to be 0.02 μg mL^{-1}, indicating the high sensitivity of the WCS-CDs-based detection system for AMK. This finding suggests that WCS-CDs can be utilized as a viable fluorescent probe for the detection of AMK.

In order to evaluate the performance of the method more comprehensively, a detailed comparison was made with other reported assays. Table 1 summarizes the detection range, and LOD of the different assays. As demonstrated in Table 1, the WCS-CDs method exhibits a low detection limit (0.02 μg mL^{-1}) and a wide detection range (1.5–21.5 μg mL^{-1}). These

Table 1 Comparison on the analytic parameters of the previous methods for AMK

Method	Detection range	LOD	References
Gallium-organic framework luminescent sensor	0–5.71 mg L^{-1}	2.27 μg L^{-1}	61
MA-Au NPs colorimetric sensor	0.03–0.13 g L^{-1}	2.8 mg L^{-1}	62
HPLC-CL	0.2–2.68 g L^{-1}	0.66 mg L^{-1}	63
WCS-CDs fluorescent probe	1.5–21.5 μg mL^{-1}	0.02 μg mL^{-1}	This work

Table 2 Effects of various amino acids interferential substances on the WCS-CDs–AMK system

Interferential substances	Concentration (μg mL^{-1})	Relative error (%)
L-Arginine	40	2
DL-Arginine	40	4
L-Cysteine	40	1
L-Cystine	40	5
L-*tert*-Leucine	40	5
Kanamycin	40	4
Spectinomycin	40	2
Penicillin–streptomycin–gentamicin solution	40	5
Neomycin sulfate	40	4

advantages enhance the reliability, practicality, and cost-effectiveness of the method for amikacin detection.

Tolerance to interferential substances

In order to verify the anti-interference capability of the detection system, a series of common amino acids and other aminoglycoside antibiotics were selected as interferents in the anti-interference test. The outcomes of this investigation are presented in Table 2. The detection of AMK was found to be largely unaffected by the presence of high concentrations of amino acids (40 μg mL^{-1}), with a relative error margin of less than 5%.

Detection of AMK in actual samples

In the subsequent phase of the study, the application ability of the detection system was explored in real samples (Table 3). Human serum, Lake water, and tap water were used as the actual samples to assess the AMK detection capability at varying concentrations. The outcomes demonstrated a recovery rate ranging from 95.58% to 105.63%, with a relative standard deviation not exceeding 3%. This result further reinforces the reliability and precision of the developed detection method.

Cell viability

To further explore the possibility of the system entering the biological environment, the cytotoxicity of the WCS-CDs was determined by MTT assay. The BEAS2B cells and A549 cells were utilized as cell models, and Fig. 8 showed that the survival rate of BEAS2B cells was more than 80% at a concentration of less than 30 μg mL^{-1}, and the survival rate of A549 cells was even more than 90%. This proved that the toxic effect of WCS-CDs on cells is negligible at a concentration of less than 30 μg mL^{-1}, thereby substantiating the WCS-CDs' high biocompatibility as a fluorescent probe. Therefore, the WCS-CDs can be potentially used as a safe fluorescent nanoprobe in biological areas and medical research.

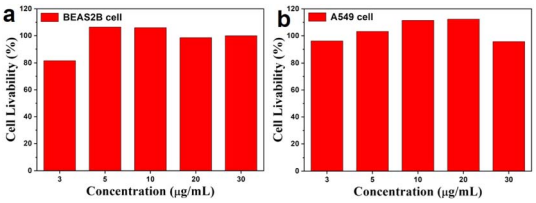

Fig. 8 (a) The BEAS2B cell livability of incubated at different WCS-CDs concentrations; (b) the A549 cell livability of incubated at different WCS-CDs concentrations.

Cell imaging

Given their robust fluorescence characteristics and low cytotoxicity, the ability of WCS-CDs to penetrate cells was evaluated using fluorescence microscopy at various excitation wavelengths. BMDM cells were employed as a model to assess the potential of WCS-CDs for intracellular bioimaging. Fig. 9

Table 3 WCS-CDs–AMK system assay in actual samples

Medium	Amikacin concentration (μg mL^{-1})		Recovery (%)	Relative standard deviation (%) ($n = 7$)
	Added	Found (mean ± SD)		
Serum	2	1.91 ± 0.03	95.58	1.55
	8	8.06 ± 0.21	100.69	2.59
	14	14.09 ± 0.11	100.62	0.81
Tap water	2	1.99 ± 0.06	99.45	3.15
	8	8.08 ± 0.23	100.95	2.87
	14	13.82 ± 0.42	98.69	3.10
Lake water	2	1.99 ± 0.04	99.69	2.04
	8	8.34 ± 0.21	104.28	2.53
	14	14.79 ± 0.47	105.63	3.16

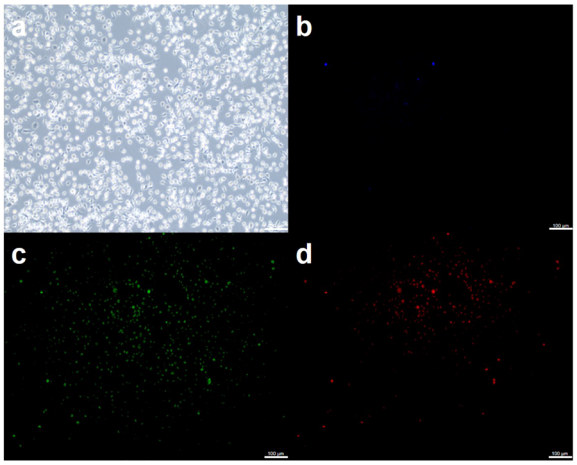

Fig. 9 (a) Brightfield image of BMDM cells; (b) blue light of WCS-CDs-stained BMDM cells; (c) green light of WCS-CDs-stained BMDM cells; (d) red light of WCS-CDs-stained BMDM cells.

illustrates the white light and fluorescence microscopy images of BMDM cells stained with WCS-CDs. Compared to the white light image, blue, green, and red fluorescence were observed within the intracellular regions of the BMDM cells. Fluorescent microscopy images revealed that WCS-CDs can successfully transfer into BMDM cells. Hence, the WCS-CDs can be used for *in vitro* cell imaging to widen the application range of WCS-CDs.

Conclusions

In conclusion, water caltrop shell-derived carbon dots (WCS-CDs) exhibiting down-conversion fluorescent properties were synthesized *via* a one-step hydrothermal process. The synthesized WCS-CDs exhibited strong photoluminescence emission, significant resistance to photobleaching, and stability against interfering substances, making them suitable as fluorescent probes for the quantitative detection of amikacin. This is achieved through the quenching of the WCS-CDs' fluorescence, which offers a broad linear detection range and a low detection limit. The biocompatibility of the synthesized WCS-CDs was confirmed through cell viability assays.[64]

Data availability

Data will be made available on request.

Author contributions

Yi Zhang: conceptualization, methodology, investigation, writing-original draft, funding acquisition. Ping Dong: methodology, data curation. Xin Chen: investigation, data curation. Jin Wang: investigation, data curation. Yun Zhang: project administration, supervision, funding acquisition. Bowen Liu: writing-review & editing, project administration, supervision, funding acquisition.

Conflicts of interest

There are no conflicts to declare.

Acknowledgements

This work was supported by Higher Education Institutions in Henan Province (No. 25B330001), the National Natural Science Foundation of China (No. 32271472), the 111 Project (No. D20036), and by the start-up fund from Xinxiang Medical University (Grant No. 201905).

References

1 Q. K. Nguyen, D. T. Nguyen, T. M. A. Pham, B. Pham, T. A. H. Nguyen, T. D. Pham, S. Sharma, D. T. Pham, R. R. Gangavarapu and T. N. M. Pham, *Spectrochim. Acta, Part A*, 2024, **305**, 123466.
2 A. Raut, D. Sharma and V. Suvarna, *Crit. Rev. Anal. Chem.*, 2022, **52**, 375–391.
3 A. Motos, H. Yang, G. Li Bassi, M. Yang, A. Meli, D. Battaglini, R. Cabrera, J. Bobi, F. Pagliara, G. Frigola, M. Camprubí-Rimblas, L. Fernández-Barat, M. Rigol, A. Ferrer-Segarra, K. Kiarostami, D. Martinez, D. P. Nicolau, A. Artigas, P. Pelosi, J. Vila and A. Torres, *Crit. Care*, 2023, **27**, 60.
4 M. Alizadeh, M. Amiri and A. Bezaatpour, *Curr. Drug Delivery*, 2021, **18**, 761–769.
5 M. Rutschmann, N. Redinger, U. E. Schaible and C. Feldmann, *J. Mater. Chem. B*, 2023, **11**, 5460–5468.
6 H. Luo, L. Xu and Y. Chen, *Diagn. Microbiol. Infect. Dis.*, 2023, **106**, 115956.
7 A. Maxwell, V. Ghate, J. Aranjani and S. Lewis, *Life Sci.*, 2021, **284**, 119883.
8 M. S. Ramirez and M. E. Tolmasky, *Molecules*, 2017, 22.
9 M. Bassetti, A. Vena, A. Russo and M. Peghin, *Drugs*, 2020, **80**, 1309–1318.
10 J. F. Ovalles, R. Brunetto Mdel and M. Gallignani, *J. Pharm. Biomed. Anal.*, 2005, **39**, 294–298.
11 Y. Chen, Y. Wang, B. Guo, Y. Fan, H. Wu, X. Li, Y. Li, X. Huang, M. Chen, X. Liu and J. Zhang, *J. Chromatogr. B:Anal. Technol. Biomed. Life Sci.*, 2023, **1220**, 123592.
12 J. F. Ovalles, M. Gallignani, M. R. Brunetto, R. A. Rondón and C. Ayala, *J. Pharm. Anal.*, 2014, **4**, 125–131.
13 K. Chan, W. Wang, K. R. Ledesma, T. Yin and V. H. Tam, *Bioanalysis*, 2020, **12**, 445–454.
14 C. Balan, L. C. Pop and M. Baia, *Spectrochim. Acta, Part A*, 2019, **214**, 79–85.
15 H. W. Kroto, *Angew Chem. Int. Ed. Engl.*, 1992, **31**, 111–129.
16 S. Iijima, *Nature*, 1991, **354**, 56–58.
17 K. S. Novoselov, A. K. Geim, S. V. Morozov, D. Jiang, Y. Zhang, S. V. Dubonos, I. V. Grigorieva and A. A. Firsov, *Science*, 2004, **306**, 666–669.
18 X. Xu, R. Ray, Y. Gu, H. J. Ploehn, L. Gearheart, K. Raker and W. A. Scrivens, *J. Am. Chem. Soc.*, 2004, **126**, 12736–12737.
19 Y. P. Sun, B. Zhou, Y. Lin, W. Wang, K. A. Fernando, P. Pathak, M. J. Meziani, B. A. Harruff, X. Wang, H. Wang,

P. G. Luo, H. Yang, M. E. Kose, B. Chen, L. M. Veca and S. Y. Xie, *J. Am. Chem. Soc.*, 2006, **128**, 7756–7757.
20 R. Dhiman, J. Kumar and M. Singh, *Anal. Sci.*, 2024, **40**, 1387–1396.
21 W. Gao, J. He, L. Chen, X. Meng, Y. Ma, L. Cheng, K. Tu, X. Gao, C. Liu, M. Zhang, K. Fan, D. W. Pang and X. Yan, *Nat. Commun.*, 2023, **14**, 160.
22 Q. Zhang, R. Wang, B. Feng, X. Zhong and K. K. Ostrikov, *Nat. Commun.*, 2021, **12**, 6856.
23 Y. Liu, H. Liu, S. Guo, Y. Zhao, J. Qi, R. Zhang, J. Ren, H. Cheng, M. Zong, X. Wu and B. Li, *Carbohydr. Polym.*, 2024, **323**, 121445.
24 A. Kolanowska, G. Dzido, M. Krzywiecki, M. M. Tomczyk, D. Łukowiec, S. Ruczka and S. Boncel, *ACS Omega*, 2022, **7**, 41165–41176.
25 G. Zuo, J. Hu, Y. Wang, A. Xie and W. Dong, *Luminescence*, 2019, **34**, 759–766.
26 F. Guo, Q. Li, X. Zhang, Y. Liu, J. Jiang, S. Cheng, S. Yu, X. Zhang, F. Liu, Y. Li, G. Rose and H. Zhang, *Int. J. Nanomed.*, 2022, **17**, 6621–6638.
27 Y. Y. Liu, N. Y. Yu, W. D. Fang, Q. G. Tan, R. Ji, L. Y. Yang, S. Wei, X. W. Zhang and A. J. Miao, *Nat. Commun.*, 2021, **12**, 812.
28 L. Ai, Z. Song, M. Nie, J. Yu, F. Liu, H. Song, B. Zhang, G. I. N. Waterhouse and S. Lu, *Angew Chem. Int. Ed. Engl.*, 2023, **62**, e202217822.
29 S. Ding, P. Tan, J. Wen, T. Li and W. Wang, *Sci. Total Environ.*, 2022, **814**, 152745.
30 H. Zhang, Y. Gao, Y. Jiao, W. Lu, S. Shuang and C. Dong, *Analyst*, 2020, **145**, 2212–2218.
31 B. Peng, J. Xu, M. Fan, Y. Guo, Y. Ma, M. Zhou and Y. Fang, *Anal. Bioanal. Chem.*, 2020, **412**, 861–870.
32 W. Li, Z. Chen, H. Yu, J. Li and S. Liu, *Adv. Mater.*, 2021, **33**, e2000596.
33 L. Sun, R. Zhang, T. Zhang, X. Liu, Y. Zhao, M. Yang, H. Cheng, Q. Zhang, Y. Zhang, X. Wu and B. Li, *Biomed. Mater.*, 2023, **18**, 042004.
34 V. Manikandan and N. Y. Lee, *Environ. Res.*, 2022, **212**, 113283.
35 Y. Hu, J. Wen, D. Li, Y. Li, M. Alheshibri, M. Zhang, L. Shui and N. Li, *Spectrochim. Acta, Part A*, 2023, **303**, 123149.
36 J. Wu, J. H. Lei, M. Li, A. Zhang, Y. Li, X. Liang, S. C. de Souza, Z. Yuan, C. Wang, G. Chen, T. M. Liu, C. X. Deng, Z. Tang and S. Qu, *Adv. Sci.*, 2024, **11**, e2404702.
37 S. Dai, L. Yao, L. Liu, J. Cui, Z. Su, A. Zhao and P. Yang, *Acta Biomater.*, 2024, **186**, 454–469.
38 X. Dong, Y. Liu, A. F. Adcock, K. Sheriff, W. Liang, L. Yang and Y. P. Sun, *Int. J. Mol. Sci.*, 2024, **25**, 2196.
39 Y. Najmalden Ghaibullah Ghaibullah, E. Foto, N. Ozdemir, F. Zilifdar Foto, G. Arslan and I. Sargin, *Int. J. Biol. Macromol.*, 2024, **257**, 128586.
40 W. Dos Santos de Almeida, L. M. Gomes Abegão, A. Vinicius Silva Alves, J. de Oliveira Souza Silva, S. Oliveira de Souza, F. d'Errico and E. Midori Sussuchi, *Chemistry*, 2024, **30**, e202303771.
41 Q. Wang, X. He, J. Mao, J. Wang, L. Wang, Z. Zhang, Y. Li, F. Huang, B. Zhao, G. Chen and H. He, *Molecules*, 2024, **29**, 4211.
42 Y. Tang, L. Lu, X. Zang, B. Wang and X. Ye, *ChemSusChem*, 2023, **16**, e202300357.
43 J. Kim, S. D. Han, B. Koo, S. H. Lee and J. Yang, *Polymers*, 2023, **15**, 4373.
44 X. Sun, Q. Lei, Q. Chen, D. Song, M. Zhou, H. Wang and L. Wang, *Molecules*, 2024, **29**, 1238.
45 C. H. Hsu, Z. B. Pan, C. R. Chen, M. X. Wei, C. A. Chen, H. P. Lin and C. H. Hsu, *ACS Omega*, 2020, **5**, 10626–10632.
46 T. Tian, Y. He, Y. Ge and G. Song, *Sens. Actuators, B*, 2017, **240**, 1265–1271.
47 G. Magdy, A. F. Abdel Hakiem, F. Belal and A. M. Abdel-Megied, *Food Chem.*, 2021, **343**, 128539.
48 Y. Hu, Z. Gao and J. Luo, *Food Chem.*, 2021, **335**, 127677.
49 R. Atchudan, T. Edison and Y. R. Lee, *J. Colloid Interface Sci.*, 2016, **482**, 8–18.
50 S. Narimani, N. Samadi and E. Delnavaz, *Anal. Sci.*, 2024, **40**, 1521–1528.
51 Y. M. Yang, Y. Yan, J. Y. Zhou, C. Z. Huang, S. J. Zhen and L. Zhan, *Anal. Sci.*, 2024, **40**, 511–518.
52 Y. Huang, X. Si, M. Han and C. Bai, *Molecules*, 2022, 27.
53 V. Țucureanu, A. Matei and A. M. Avram, *Crit. Rev. Anal. Chem.*, 2016, **46**, 502–520.
54 C. Zou, Z. Liu, X. Wang, H. Liu, M. Yang, D. Huo and C. Hou, *Spectrochim. Acta, Part A*, 2022, **265**, 120346.
55 Y. Dong, H. Pang, H. B. Yang, C. Guo, J. Shao, Y. Chi, C. M. Li and T. Yu, *Angew Chem. Int. Ed. Engl.*, 2013, **52**, 7800–7804.
56 T. Jiang, J. Huang, G. Ran, Q. Song and C. Wang, *Anal. Sci.*, 2023, **39**, 325–333.
57 R. Atchudan, T. Edison, K. R. Aseer, S. Perumal, N. Karthik and Y. R. Lee, *Biosens. Bioelectron.*, 2018, **99**, 303–311.
58 Y. Shi, Y. Xia, M. Zhou, Y. Wang, J. Bao, Y. Zhang and J. Cheng, *J. Nanobiotechnol.*, 2024, **22**, 88.
59 R. Atchudan, T. J. I. Edison, S. Perumal, N. Muthuchamy and Y. R. Lee, *Fuel*, 2020, **275**, 117821.
60 T. N. Edison, R. Atchudan, J. J. Shim, S. Kalimuthu, B. C. Ahn and Y. R. Lee, *J. Photochem. Photobiol., B*, 2016, **158**, 235–242.
61 Y. Xie, Z. H. Jiao, J. Dong, S. L. Hou and B. Zhao, *Inorg. Chem.*, 2023, **62**, 5168–5175.
62 S. Zhu, D. Zuo, Q. Shi, J. Yuan and B. Wang, *Anal. Methods*, 2024, **16**, 7063–7072.
63 J. M. Serrano and M. Silva, *J. Chromatogr. B:Anal. Technol. Biomed. Life Sci.*, 2006, **843**, 20–24.
64 S. Singh, P. Nigam, A. Pednekar, S. Mukherjee and A. Mishra, *Environ. Technol.*, 2020, **41**, 322–328.